Study on the Reliability of Electric Motor Boat Propeller Structure Due to Axial Load

Admarch Gery Haryoseno[1] and Aries Sulisetyono[1*]

[1]Department of Naval Architecture, Faculty of Marine Technology, Sepuluh Nopember Institute of Technology
*Email: sulisea@na.its.ac.id

Abstract. This study investigates the structural reliability of B-Series propellers used in electric motor-driven ships under axial loads induced by fluid flow. The distinct operating characteristics of electric propulsion systems require dedicated reliability assessment to ensure safe and efficient performance. Computational Fluid Dynamics (CFD) simulations were conducted under uniform viscous flow conditions to evaluate hydrodynamic loading, yielding a maximum axial load of 32.74 kN at a rotational speed of 1500 RPM. The resulting loads were applied in Finite Element Method (FEM) simulations to assess structural stress and deformation, with maximum values of 273.27 MPa and 5.10 mm, respectively. Structural reliability analysis was performed using probability density functions of hydrodynamic loads and aluminum alloy material strength. The results indicate a structural reliability of 99.90% at a ship speed of 10 knots, which decreases significantly to 33.31% at 20 knots. The inclusion of safety factors of 10% and 40% effectively increased reliability by 9.99% and 100%, respectively. These findings emphasize the importance of appropriate safety factors and material selection to improve the structural reliability of electric motor ship propellers under high-speed operating conditions.

Keywords: B-Series Propeller, Computational Fluid Dynamics, Electric Motor Ship, Structural Reliability, Finite Element Method.

1. Introduction

The propeller is a critical component of electric motor boat propulsion systems, directly governing thrust generation, efficiency, and operational reliability. B-Series propellers are widely adopted due to their well-documented hydrodynamic characteristics, making them suitable benchmarks for numerical and experimental studies [2]. During operation, propeller blades are subjected to complex hydrodynamic loads, primarily axial and tangential forces, which significantly affect structural integrity and service life.

Axial loads arise from thrust generation along the shaft direction and may induce high stress levels, increasing the risk of deformation or structural failure if not properly considered during design [6]. Tangential forces generated by rotational motion contribute to torque and cyclic stresses, and their interaction with axial loads further intensifies structural demands on the blades [3]. Consequently, both load components play a decisive role in determining propeller reliability.

Structural performance is commonly evaluated through pressure distribution, deformation, and equivalent stress, while material selection is essential to withstand repeated loading cycles and seawater corrosion [4]. From a hydrodynamic perspective, achieving high thrust with minimal torque remains a primary objective, governed

by parameters such as rotational speed, advance ratio, diameter, pitch ratio, and blade area ratio [11]. Therefore, propeller design must balance hydrodynamic efficiency and structural strength.

Computational Fluid Dynamics (CFD) is extensively applied to predict flow characteristics and hydrodynamic loads, whereas the Finite Element Method (FEM) is used to analyze stress distribution and deformation under axial and rotational loading. Their integration provides a comprehensive framework for fluid–structure interaction analysis, improving prediction accuracy and structural assessment [3], [12]. However, deterministic approaches cannot fully represent uncertainties in operating conditions, load variations, and material properties. Reliability-based methods have therefore been introduced to quantify failure probability and evaluate structural safety under uncertain scenarios [5].

Despite extensive research on hydrodynamic performance and structural response, limited attention has been given to the structural reliability of B-Series propellers for electric motor boats under axial loading. Accordingly, this study investigates the structural reliability of a B-Series propeller by integrating CFD and FEM to evaluate hydrodynamic loads, stress distribution, and deformation across varying operating speeds, followed by reliability analysis to estimate failure probability and assess safety margins. This work contributes to the development of reliable and efficient propeller designs for electric marine propulsion, supporting safe maritime operations [15].

2. Literature Review

Structural reliability of marine propellers is critical for electrically powered vessels due to high axial loads and complex hydrodynamic environments. Propeller performance and durability are strongly influenced by rotational speed, axial loading, and flow conditions [6], [7]. Hydrodynamic forces generated during operation directly affect propulsion efficiency and structural integrity.

To evaluate these effects, Computational Fluid Dynamics (CFD) is commonly used to predict flow behavior, while the Finite Element Method (FEM) analyzes stress and deformation on propeller blades [3]. This coupled approach enables identification of high-stress regions and potential failure locations. Reliability-based optimization further accounts for uncertainties in loading and material properties, leading to safer and optimized designs [5].

Hydrodynamic interaction between the propeller and surrounding water governs thrust generation and efficiency. Axial loads produced by pressure distribution along blade surfaces can cause deformation and accelerate material degradation if not properly considered in design. CFD is applied to determine pressure distribution and critical loading zones, whereas FEM evaluates structural responses under these loads [12], [13].

Excessive axial loading increases structural stress and wear, reducing operational lifespan. Numerical simulations are therefore widely adopted to model fluid–structure interaction, assess load variations, and optimize propeller geometry under different operating conditions. These approaches contribute to improved efficiency, reliability, and long-term durability of marine propellers [11], [14].

3. Methodology

The overall methodology of this study is illustrated in Figure 1, showing the integration of Computational Fluid Dynamics (CFD), Finite Element Method (FEM), and reliability analysis to evaluate the structural performance of a B-Series propeller. The process begins with collecting propeller geometry and material properties, followed by 3D modeling and meshing, hydrodynamic simulation, structural analysis, and probabilistic reliability evaluation.

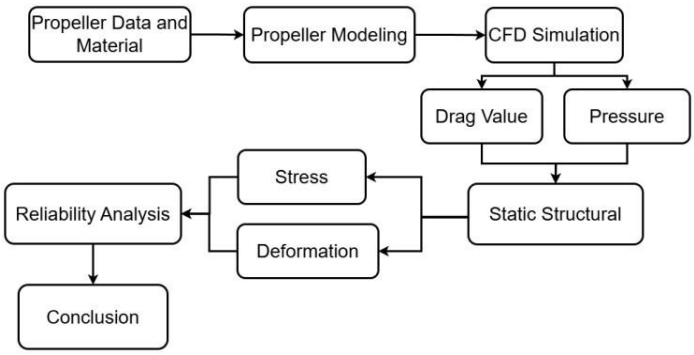

Figure 1 Flowchart

Propeller dimensions and material data are used to construct a three-dimensional model, which is discretized into finite elements. Mesh refinement is applied on blade surfaces to improve numerical accuracy, particularly in capturing pressure gradients and stress concentrations. CFD simulations are performed in ANSYS Fluent to obtain pressure distribution and axial loads under realistic operating conditions, including inflow velocity and rotational speed. These hydrodynamic loads are subsequently transferred to FEM for structural assessment, enabling evaluation of stress and deformation caused by axial loading [12].

Table 1 Principal Dimensions Propeller

PRINCIPAL DIMENSIONS		
Nama	**Dimension**	**Unit**
Diameter	0.7	M
Pitch	2.2	M
Blade Area	0.056	M^2
Number of Blades	4	-

To account for uncertainties in loading and material properties, a probabilistic framework is adopted. Axial loads are represented using probability density functions (PDFs), while material variability is obtained from tensile test data. Structural failure is defined when applied stress exceeds material strength, and failure probability is determined from the overlap of load and strength distributions. Table 1 summarizes the principal propeller dimensions, while Figure 2 presents the 3D geometry used for numerical analysis. Full-scale simulations are conducted to ensure realistic representation of operational conditions.

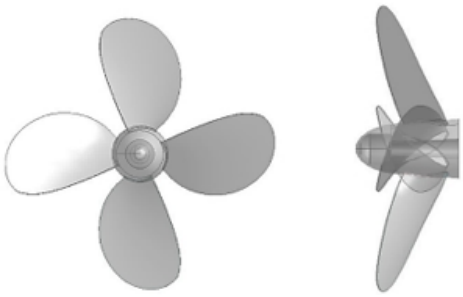

Figure 2 Propeller Design

3.1. CFD Simulation

The CFD simulation is performed to analyze the hydrodynamic behavior of the marine propeller at ten rotational speeds ranging from 1050 to 1500 rpm, representing typical operating conditions of electric motor boats. The analysis focuses on flow characteristics and pressure distribution on the propeller blades.

The simulations employ the Finite Volume Method (FVM) to discretize the Navier–Stokes equations, ensuring mass and momentum conservation [3]. Turbulence is modeled using the standard k–ε model, which is widely applied for submerged marine propellers due to its robustness in predicting turbulent flows with significant pressure gradients [2], and its suitability for steady operating conditions.

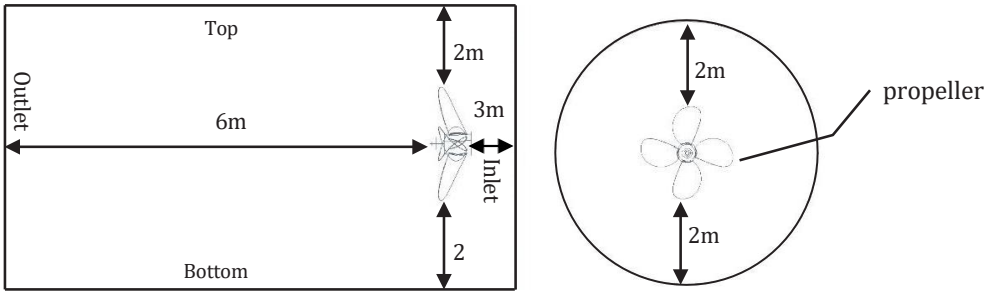

Figure 3 Boundary Condition

Pressure distribution on the blades is obtained by solving the momentum equations while considering fluid density and viscosity. Boundary conditions include velocity inlet, pressure outlet, and no-slip walls on the propeller and domain surfaces. The resulting pressure data are transferred to FEM for structural analysis, establishing fluid–structure coupling.

The computational domain and boundary conditions are shown in Figure 3, with the propeller placed 3 m from the inlet, 6 m from the outlet, and 2 m from surrounding boundaries to reduce numerical interference, following previous recommendations [6]. A mesh independence study yields an optimal grid of 27,347 elements (Table 2). Local mesh refinement is applied near blade surfaces, especially at leading and trailing edges, as illustrated in Figure 4, to capture high pressure gradients efficiently.

Table 2 Grid Independence Study

Grid Independence Study			
Element size	**Number of Mesh**	**Max Stress, MPa**	**Gap**
10 mm	27347	62.634	3%
20 mm	10862	64.332	6%
30 mm	8393	68.682	2%
40 mm	6874	67.242	-

The CFD results provide detailed pressure distributions required to evaluate hydrodynamic performance and identify high-load regions, including potential cavitation zones. These pressure fields serve as input for subsequent FEM-based stress and deformation analyses, following established numerical procedures [4].

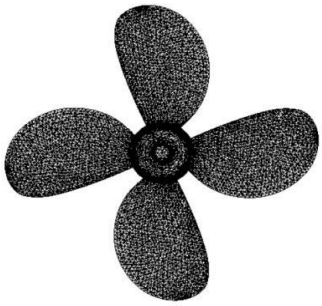

Figure 4 Meshing

3.2. Static Structural Analysis

In the Static Structural analysis in Figure 5, Static structural analysis is performed using FEM to evaluate stress distribution and deformation under hydrodynamic loading. Fixed support is applied at the front hub surface (point C), representing shaft attachment, while axial load is applied at the rear hub (point B). CFD-derived pressure is imposed on the blade surface (point A) to represent fluid–structure interaction [1].

The von Mises criterion is employed to assess equivalent stress, assuming linear elastic material behavior based on Hooke's law. This coupled CFD–FEM approach enables identification of critical regions susceptible to structural failure under axial loading [15].

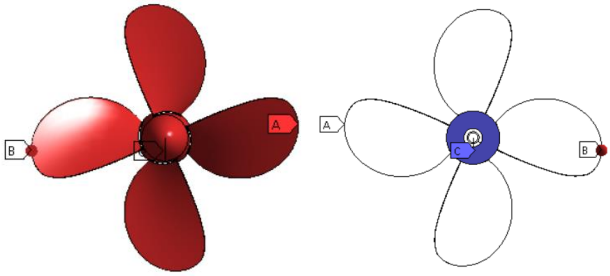

Figure 5 Static Structural

3.3. Strength of Material

Structural resistance is evaluated using yield strength as the primary failure criterion [9]. Aluminum is selected as the propeller material, with mechanical properties obtained from tensile test results (Table 3) [8]. The results show consistent yield and ultimate tensile strengths across different thicknesses, with maximum elongation of approximately 1.5%, indicating limited ductility. Material variability is incorporated into the probabilistic framework to account for uncertainty in structural strength.

Table 3 Tensile properties of aluminium samples from different thicknesses and heat treatments [Kim et al., 2021]

Wedge Thickness (mm)	YS (MPa)	UTS (MPa)	Elongation (%)	BHN
14	465	473	1.0	144
33	396	402	0.9	124
21	453	453	0.8	138
25	450	480	1.5	140
30	428	450	1.2	142
40	360	360	0.7	132
43	343	355	0.9	132
47	327	332	0.8	120
18	446	446	0.8	145
37	370	370	0.8	126

3.4. Reliability Analysis

This study applies a reliability-based approach to evaluate propeller structural integrity under axial loading. A probabilistic method is adopted using two stochastic variables: structural strength and applied load. Two Probability Density Functions (PDFs), representing strength $f_r(R_0)$ and load $f_s(S)$, are defined as shown in Figure 6, where R_0 and S are expressed in stress units. The probability of failure is determined from the overlap region of these PDFs, corresponding to the joint probability density function [1].

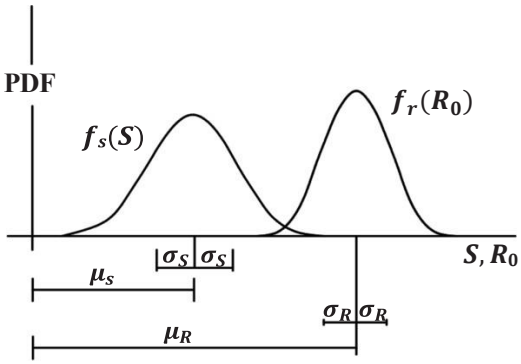

Figure 6 PDF Variabel R_O dan S

A simple function, $g(S, R_0)$, is defined to represent the limit state function, which describes the safety margin SM, as the difference between the structural strength $f_r(R_0)$ and the applied load $f_s(S)$, expressed in Equation (1).

$$SM = g(S, R_0) = f_r(R_0) - f_s(S) \quad (1)$$

Based Based on the above equation, three criteria can be identified for each value of $g(S, R_0)$ as follows:

- $g(S, R_0) < 0$, Failure region, where the structural load, $f_s(S)$, exceeds the structural strength $f_r(R_0)$.
- $g(S, R_0) > 0$, the safe area, where the load, $f_s(S)$, is less than the strength of the structure $f_r(R_0)$.
- $g(S, R_0) = 0$, the boundary area between safety and failure, where the load, $f_s(S)$, is equal to $f_r(R_0)$.

The probability of failure can be calculated by equation (2).

$$P_f = P[M = g(S, R_0) \leq 0] = \iint_{g(S,R_0)\leq 0} f_s(S) \cdot f_r(R_0)\, ds\, dR_0 \quad (2)$$

Where $f_{s,r}(S, R_0)$ is the joint probability function of $f_r(R_0)$ and $f_s(S)$, and the limits of the integral area encompass all values of R_0 and S, where M is non-positive, indicating an unsafe condition. In the case where the statistical strength and structural load are independent, the probability of failure is expressed in Equation (3).

$$P_f = \boldsymbol{\phi}(-\beta) \quad (3)$$

Where $\boldsymbol{\phi}(\cdot)$ is the standard normal cumulative distribution function and β is the safety index, which can be calculated by equation (4), where μ is the average, and σ is the standard deviation.

$$\beta = \frac{\mu_{R_0} - \mu_s}{\sqrt{\sigma {R_0}^2 + \sigma s^2}} \quad (4)$$

The probability of structural failure (P_f) in some cases involving many variables can be calculated using the Monte Carlo simulation method [8]. Furthermore, the reliability of the structure (R) is determined by equation (5).

$$R = 1 - Pf \quad (5)$$

4. Results and Discussion

Structural reliability of the propeller under axial loads at ten different rotational speeds was evaluated using coupled CFD and static structural FEM analyses. The results include pressure distribution, stress, and deformation, which are discussed in the following subsections.

4.1. Pressure Distribution dan Axial Drag Analysis

Figure 7 shows the pressure distribution from CFD simulations at ten rotational speeds under constant inflow velocity. High-pressure regions appear mainly at the leading edge near the blade tip, while low pressure is observed toward the trailing edge and mid-span. As listed in Table 4, both minimum and maximum pressures increase with rotational speed, ranging from 0.026–0.041 MPa at 1050 RPM to 0.043–0.066 MPa at 1500 RPM. This pressure gradient governs the axial load acting on the blades and is critical for structural reliability assessment [11].

Table 5 presents axial drag forces at a ship speed of 5.14 m/s, increasing from 10.3 kN at 1050 RPM to 19.9 kN at 1500 RPM. These results confirm that higher rotational speeds generate greater axial loads, increasing the potential for stress concentration and structural degradation, consistent with previous studies [13].

Table 4 Pressure Data Table

RPM	Minimum (Mpa)	Maximum (Mpa)
1050	0.026031	0.04129
1100	0.0290164	0.0443551
1150	0.0311521	0.0492308
1200	0.0328566	0.0518323
1250	0.0344271	0.0542286
1300	0.0360817	0.059595
1350	0.037105	0.0581774
1400	0.0393519	0.0614345
1450	0.0411436	0.0639996
1500	0.0426101	0.0660518

Table 5 Axial Drag

Rpm	Axial Drag (N)	Vs(m/s)	ω
1050	19406.6	8.084	0.573
1100	23750.4	8.099	0.576
1150	23845.5	8.216	0.598
1200	24598.6	8.417	0.638
1250	25918.6	8.624	0.678
1300	27309.8	8.714	0.695
1350	27925.3	9.020	0.755
1400	30061.2	9.226	0.795
1450	31542.0	9.389	0.827
1500	32743.6	2.267	0.559

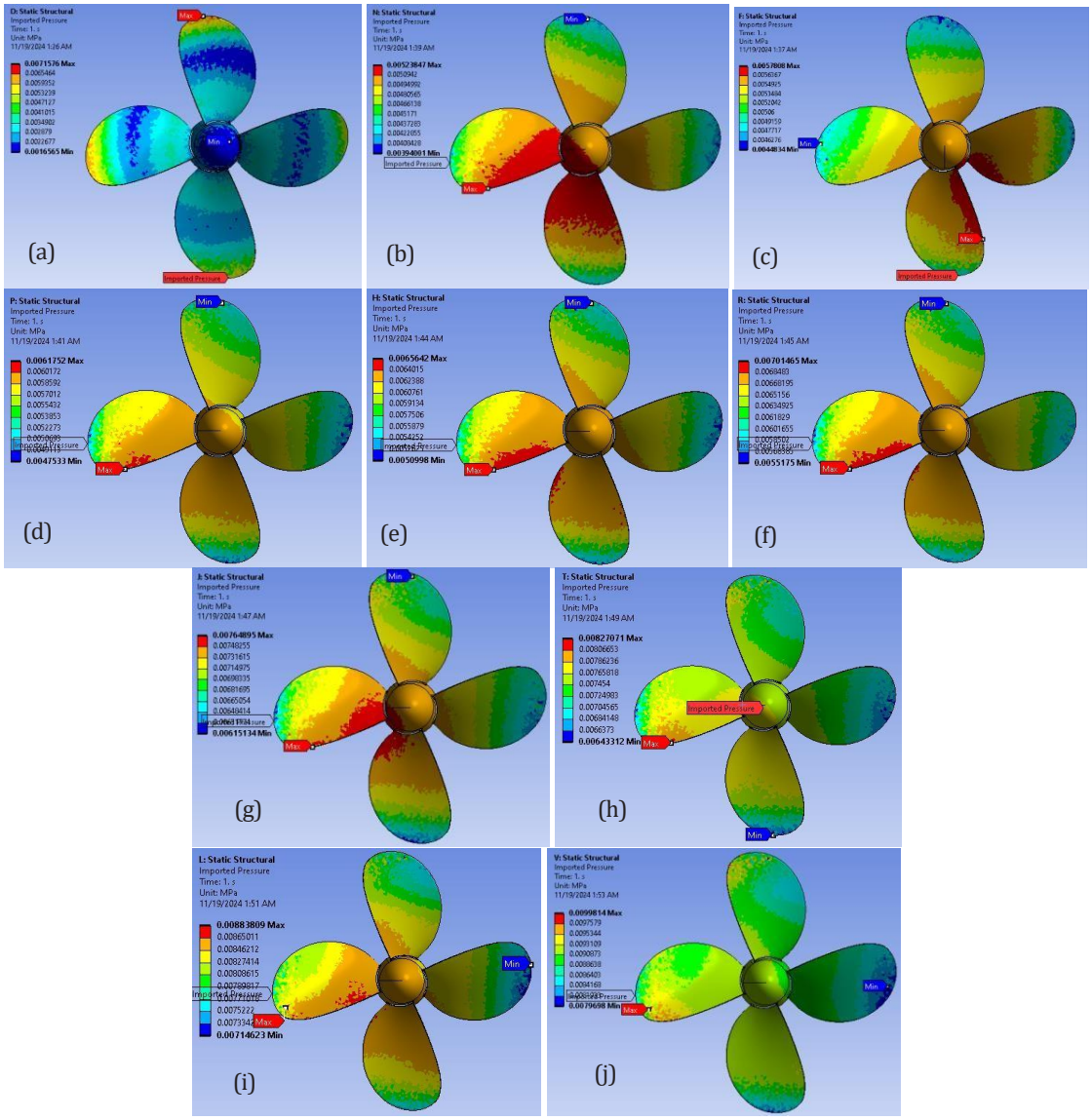

Figure 7 Imported Pressure by (a) 1050 Rpm, (b) 1100 Rpm, (c) 1150 Rpm, (d) 1200 Rpm, (e) 1250 Rpm, (f) 1300 Rpm, (g) 1350 Rpm, (h) 1400 Rpm, (i) 1450 Rpm, (j) 1500 Rpm

4.2. Stress Distribution Analysis

Static structural FEM analysis was performed using axial loads obtained from CFD to evaluate von Mises stress distribution on the propeller blades. Figure 8 shows stress contours at different rotational speeds, where maximum stress appears mainly near the blade root and along the load transfer path toward the hub.

Stress magnitude increases with rotational speed, reflecting the rise in axial force and bending moment. As listed in Table 6, the maximum von Mises stress reaches 125.36 MPa at 1500 RPM, representing the most critical operating condition. These results highlight the importance of stress evaluation under axial loading to ensure structural reliability during high-speed operation.

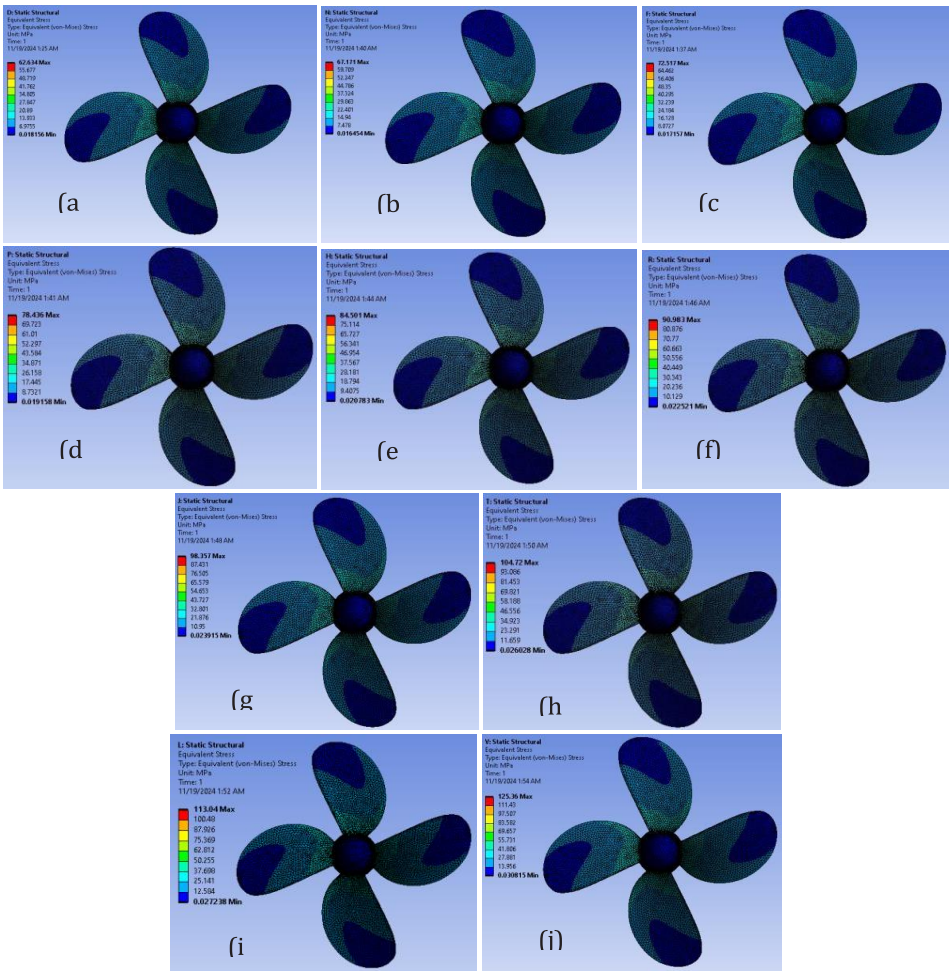

Figure 8 Equivalent Stress by (a) 1050 Rpm, (b) 1100 Rpm, (c) 1150 Rpm, (d) 1200 Rpm, (e) 1250 Rpm, (f) 1300 Rpm, (g) 1350 Rpm, (h) 1400 Rpm, (i) 1450 Rpm, (j) 1500 Rpm

Table 6 Stress & Deformation

RPM	Max Stress (Mpa)	Max Deformation (mm)
1050	163.84	3.0524
1100	193.16	3.5920
1150	199.40	3.7173
1200	207.26	3.8643
1250	218.00	4.0666
1300	229.20	4.2779
1350	234.94	4.3853
1400	251.54	4.6983
1450	263.56	4.9239

1500	273.27	5.1022

4.3. Deformation Structure

Figure 9 presents the deformation contours of the propeller at different rotational speeds, with maximum deformation concentrated near the blade tips. Deformation increases with rotational speed due to higher axial loads and bending effects, as summarized in Table 6. This evaluation ensures that blade displacement remains within acceptable limits to prevent geometric distortion and performance degradation. Similar trends have been reported in previous studies, highlighting the influence of rotational speed and hydrodynamic loading on propeller deformation [14].

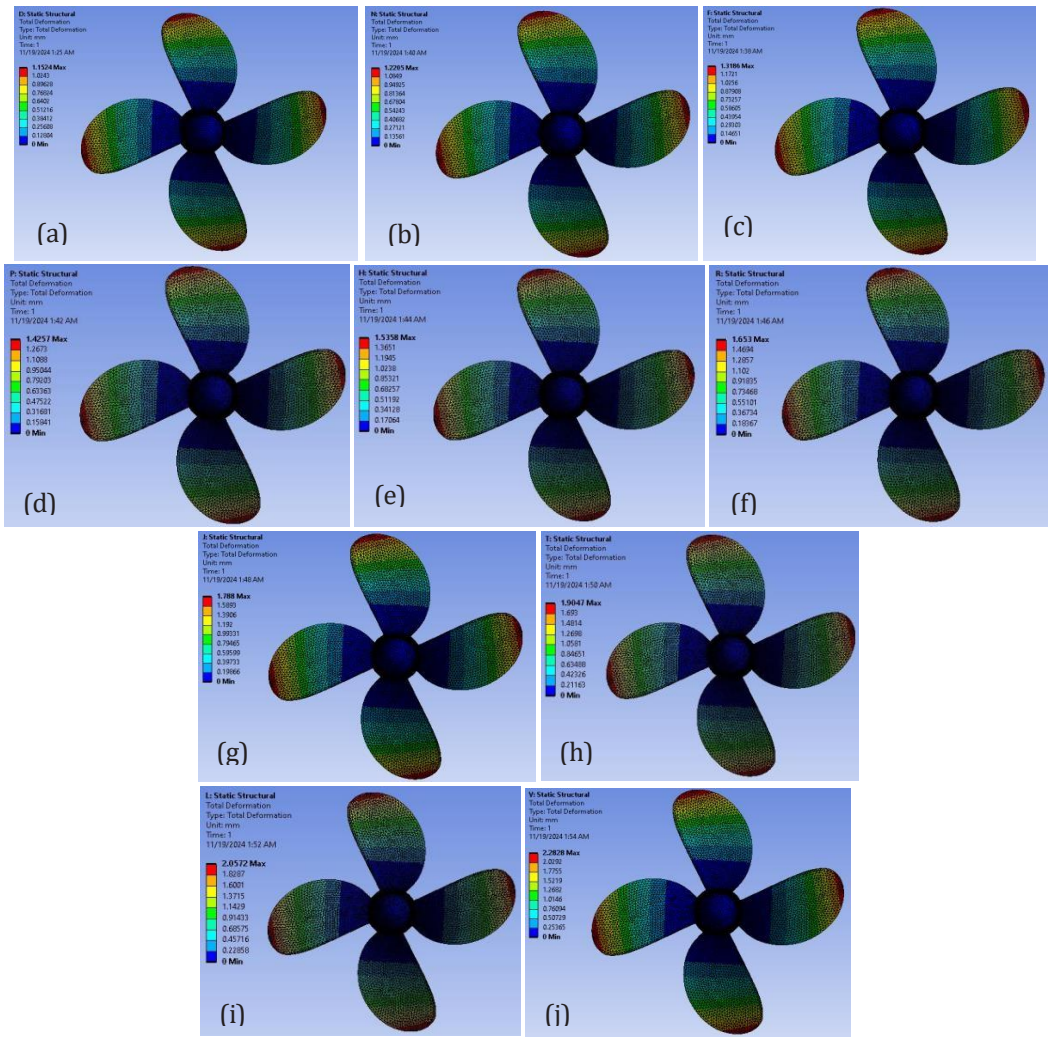

Figure 9 Total Deformation by (a) 1050 Rpm, (b) 1100 Rpm, (c) 1150 Rpm, (d) 1200 Rpm, (e) 1250 Rpm, (f) 1300 Rpm, (g) 1350 Rpm, (h) 1400 Rpm, (i) 1450 Rpm, (j) 1500 Rpm

4.4. Structural Reliability Analysis with Safety Factor

Stress results from FEM and axial loads from CFD were used to evaluate structural reliability. Mean stress and standard deviation for each rotational speed are summarized in Table 7, and stress PDFs were constructed using a normal distribution. Figure 10 presents the joint PDF between structural stress and material strength, where yield strength from tensile tests (Table 3) defines the failure limit.

Safety factors of 20% and 40% were applied (Figures 10b and 10c), showing a significant reduction in failure probability. The safety index was calculated using Equation (4) (Table 8), followed by failure probability (Equation (3)) and structural reliability R = 1 − P_f (Equation (5)). The results confirm high structural reliability, especially with safety factors applied, indicating that the propeller is suitable for axial loading conditions.

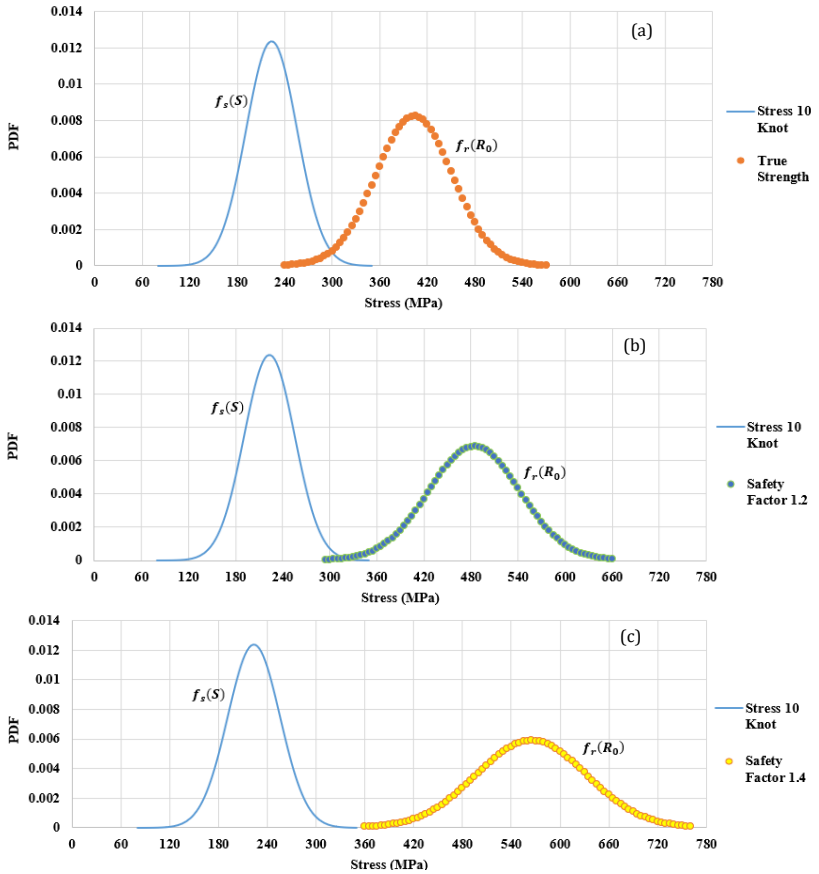

Figure 10 : Joint Probability Density Function (PDF) with Safety Factor

Table 7 : Stress of loads and compared to material strength at various safety factors.

Parameter	Stress of loads (μ_s)	Stress of Tensile Test		
		True Strength (μ_{R_0})	Safety Factor 1.2 (μ_{R_0})	Safety Factor 1.4 (μ_{R_0})
Mean (μ)	223.42	403.8	484.56	565.32
Sigma (σ)	32.23	48.36	58.03	67.70

Table 8 : Analysis of safety index, failure probability, and structural reliability with safety factors.

Parameter	True Strength	Safety Factory	Safety Factor 1.4
Safety Index (β)	3.104	3.934	4.561
Failure (P_f)	0.10%	0.004%	0.00%
Reliability ($1 - p_f$)	99.90%	99.996%	100%

4.5. Structural Reliability Analysis with Various Loads

Figure 11 shows the joint PDF between structural stress and material strength under axial loading at inlet velocities of 10, 15, and 20 knots. Increasing inlet velocity intensifies hydrodynamic loads, resulting in higher stress levels. The corresponding mean and standard deviation values are summarized in Table 9 and used to calculate the safety index Table 10 via Equation (4), followed by failure probability Equation (3) and structural reliability Equation (5).

The results indicate that structural reliability decreases with increasing ship speed due to higher hydrodynamic loading. Operation above 15 knots significantly raises failure risk; therefore, a maximum speed of 15 knots is

recommended to maintain acceptable reliability. The use of materials with higher yield strength than aluminum is also suggested to improve propeller durability under elevated loading conditions.

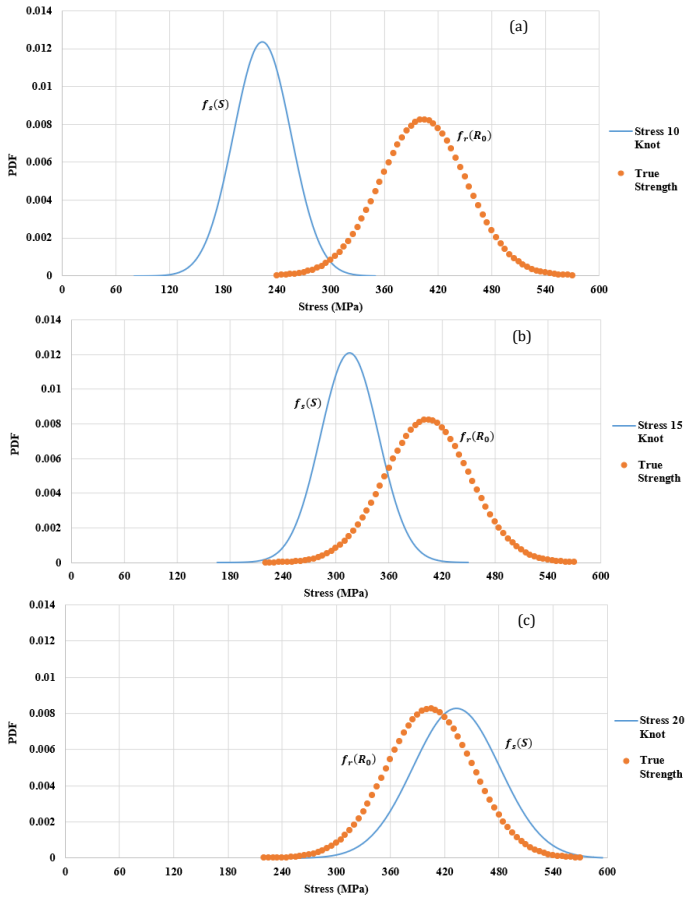

Figure 11 : Curve Probability Density Function (PDF) with Various Load

Table 9 : Stress of Loads with Various Flow Speed and Tensile Test

	Stress of Loads with Various Flow Speed			**Stress of Tensile Test**
Parameter	**10 Knot (μ_s)**	**15 Knot (μ_s)**	**20 Knot (μ_s)**	**True Strength (μ_{R_0})**
Mean (μ)	223.417	315.272	433.244	403.8
Sigma (σ)	32.227	33.002	48.154	48.357

Table 10 : Analysis of safety index, failure probability, and reliability with Various Flow Speed

Parameter	**Stress 10 Knot**	**Stress 15 Knot**	**Stress 20 Knot**
Safety Index (β)	3.104077	1.51213643	-0.4314569
Failure (p_f)	0.10%	6.525%	66.693%
Reliability ($1 - p_f$)	99.90%	93.475%	33.307%

5. Conclusion

This This study investigated the structural reliability of an electric motor boat propeller subjected to axial loads using an integrated approach combining Computational Fluid Dynamics (CFD), Finite Element Method (FEM), and reliability analysis. CFD simulations were employed to evaluate hydrodynamic loads at various propeller rotational speeds, while FEM was used to assess the resulting stress and deformation responses. Reliability analysis was subsequently conducted to quantify failure probability and the influence of safety factors under different operating conditions.

The CFD results indicate that axial loads increase with rising propeller rotational speed, reaching a maximum of 32.74 kN at 1500 RPM. Correspondingly, FEM analysis at this condition produced a maximum von Mises stress of 273.27 MPa and a deformation of 5.10 mm. Reliability evaluation across all rotational speed variations yielded a low failure probability of 0.1%, corresponding to a reliability level of 99.90%. The application of safety factors of 10% and 40% further improved the reliability, increasing it by 9.99% and up to full reliability, respectively.

Additional reliability analysis considering variations in ship speed revealed that structural reliability remained high at 10 knots (99.90%) but decreased significantly to 33.31% at 20 knots due to increased hydrodynamic loading. These findings demonstrate that higher operational speeds substantially reduce structural reliability. Therefore, it is recommended to limit ship speed to acceptable operational ranges and consider alternative propeller materials with higher yield strength than aluminum to enhance structural durability and reliability under elevated loading conditions.

References

[1] Truelock, D., Lavroff, J., Pearson, D., Czaban, Z., Luo, H., Wang, F., ... & Nicholls-Lee, R. (2022, September). Committee v. 5: Special vessels. In International Ship and Offshore Structures Congress (p. D011S001R006). SNAME.

[2] Purwana A, Ariana IM, Handani DW, Wardhana W (2018) Performance and noise prediction of marine propeller using numerical simulation. IPTEK J. Proceedings Series 1:20–25.

[3] Guan G, Zhang X, Wang P, Yang Q (2022) Multi-objective optimization design method of marine propeller based on fluid-structure interaction. Ocean Eng 252:111222.

[4] Kim SW, Lee SJ, Kim DU, Kim MS (2021) Experimental investigation on tensile properties and yield strength modeling of T5 heat-treated counter pressure cast A356 aluminum alloys. Metals 11:1192.

[5] Gholinezhad H, Torabi SH (2022) Reliability-based multidisciplinary design optimization of an underwater vehicle including cost analysis. J Mar Sci Technol 27:11–26.

[6] Ortolani F, Dubbioso G, Muscari R, Mauro S, Di Mascio A (2018) Experimental and numerical investigation of propeller loads in off-design conditions. J Mar Sci Eng 6:45.

[7] Guo HP, Zou ZJ, Wang F, Liu Y (2019) Numerical investigation on the hydrodynamic characteristics of a marine propeller operating in oblique inflow. Appl Ocean Res 93:101969.

[8] Vizentin G, Vukelic G, Murawski L, Recho N, Orovic J (2020) Marine propulsion system failures—A review. J Mar Sci Eng 8:662.

[9] Iqbal M, Gafur A, Antoko B (2023) Analisis Optimalisasi Nilai Thrust, Torque, dan Efficiency Propeller B Series dan Kaplan Series pada Studi Kasus Kapal Pencalang 15 GT Menggunakan Metode CFD. In: Proceedings of the Conference on Marine Engineering and Its Application 6(1):1–6.

[10] Özsayan S, Köksal ÇS, Usta O, Çelik C, Yılmaz N, Korkut E (2022) An experimental and numerical investigation of the cavitation effects on propeller performance and erosion on DTMB-5415 propeller. In: Proceedings of the 7th International Symposium of Marine Propulsors, Wuxi, China.

[11] Marques CH, Belchior CR, Caprace JD (2019) Marine propeller parametric optimization and matching to electric motor. J Braz Soc Mech Sci Eng 41:1–11.

[12] Rochmad AN, Sulisetyono A (2024) Fluid–Structure Interaction of a Flat-Rudder Floater in N219 Floatplane Maneuvers at the Water's Surface. SpringerBriefs in Applied Sciences and Technology:21–30. https://doi.org/10.1007/978-3-031-67788-5_3.

[13] Zou, D., Zhang, J., Ta, N., & Rao, Z. (2019). Study on the axial exciting force characteristics of marine propellers considered the effect of the shaft and blade elasticity. Applied Ocean Research, 89, 141-153.

[14] Magionesi, F., Dubbioso, G., & Muscari, R. (2024). Fluid–structure interaction of a marine rudder at incidence in the wake of a propeller. Physics of Fluids, 36(6).

[15] Stambaugh, K. A. (2020). On ship structure risk and total ownership Cost management assisted by prognostic hull structure monitoring. *Delft University of Technology*.